Framework for the Mapping of the Monthly Average Daily Solar Radiation Using an Advanced Case-Based Reasoning and a Geostatistical Technique

ARTICLE *in* ENVIRONMENTAL SCIENCE & TECHNOLOGY · MARCH 2014

Impact Factor: 5.33 · DOI: 10.1021/es405293u · Source: PubMed

4 AUTHORS, INCLUDING:

Minhyun Lee
Yonsei University
17 PUBLICATIONS **63** CITATIONS
SEE PROFILE

Choongwan Koo
Purdue University
55 PUBLICATIONS **457** CITATIONS
SEE PROFILE

Taehoon Hong
Yonsei University
185 PUBLICATIONS **914** CITATIONS
SEE PROFILE

Environmental Science & Technology

Article

pubs.acs.org/est

Framework for the Mapping of the Monthly Average Daily Solar Radiation Using an Advanced Case-Based Reasoning and a Geostatistical Technique

Minhyun Lee, Choongwan Koo, Taehoon Hong,* and Hyo Seon Park

Department of Architectural Engineering, Yonsei University, Seoul, 120-749, Republic of Korea

Supporting Information

ABSTRACT: For the effective photovoltaic (PV) system, it is necessary to accurately determine the monthly average daily solar radiation (MADSR) and to develop an accurate MADSR map, which can simplify the decision-making process for selecting the suitable location of the PV system installation. Therefore, this study aimed to develop a framework for the mapping of the MADSR using an advanced case-based reasoning (CBR) and a geostatistical technique. The proposed framework consists of the following procedures: (i) the geographic scope for the mapping of the MADSR is set, and the measured MADSR and meteorological data in the geographic scope are collected; (ii) using the collected data, the advanced CBR model is developed; (iii) using the advanced CBR model, the MADSR at unmeasured locations is estimated; and (iv) by applying the measured and estimated MADSR data to the geographic information system, the MADSR map is developed. A practical validation was conducted by applying the proposed framework to South Korea. It was determined that the MADSR map developed through the proposed framework has been improved in terms of accuracy. The developed MADSR map can be used for estimating the MADSR at unmeasured locations and for determining the optimal location for the PV system installation.

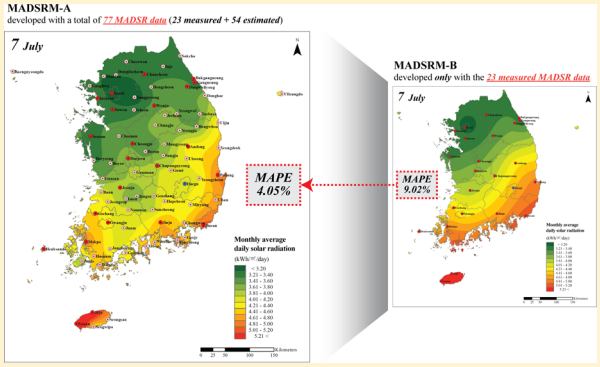

1. INTRODUCTION

To cope with climate change and air pollution, which are recognized as global problems, the United Nations Framework Convention on Climate Change (UNFCCC), which restricts greenhouse gas (GHG) emissions as a way of addressing global warming, was established in 1992.[1] In 1997, the third Conference of the Parties to the UNFCCC adopted the Kyoto Protocol, which regulated the compulsory GHG emission reduction for the developed country Parties.[2] Along with such global trends in resolving environmental issues, the South Korean government has set a 30% GHG emissions reduction as its carbon emissions reduction target to be business-as-usual by 2020.[3−6]

As part of such efforts to reduce the global GHG emissions, there is a growing interest in new renewable energy (NRE), such as photovoltaic (PV) energy, wind energy, solar heat, and biofuel.[7] The NRE market has seen consistent growth for the last ten years, thanks to the various NRE-related policies, like Feed in Tariff and Renewable Portfolio Standard. Many countries continually establish NRE policies to promote the NRE market and to reduce the NRE development costs, which have resulted in the rapid growth of NRE supplies.[8−10] In the U.S. in 2010, NRE accounted for about 10.9% of the domestic primary energy production (compared with nuclear's 11.3%), which represents a 5.6% increases from 2009. In Germany, 11% of its total final energy consumption is supplied by NRE, which accounted for 16.8% of electricity consumption, 9.8% of heat production, and 5.8% of transportation fuel consumption. Globally, the total capacity of various NRE technologies has increased at average rates from 15% to 50% annually from 2005 to 2010.[11,12]

The PV energy is considered the sustainable energy source with the highest potential among the NREs.[13] The additional installation capacity of the PV market was merely 7.2 GW in 2009, but it grew more than 2-fold to 16.6 GW in 2010.[14] As of 2011, the total installation capacity of the global PV energy went up to 40 GW, resulting in 50 TWh electricity generation per year,[15] but the amount of electricity generation from such a PV system is largely affected by the monthly average daily solar radiation (MADSR). Thus, it is important to accurately determine the MADSR for the efficient introduction of a PV system.[16−24]

In reality, however, it is difficult to measure MADSR data in all locations due to the cost, time, and measurement locations; thus, there have been many studies on estimating the MADSR at unmeasured locations.[25−32] As with the MADSR estimation model, it is necessary to determine the MADSR distribution by region based on the MADSR map. Recently, data visualization has become a powerful tool for effective decision making. As

Received: December 3, 2013
Revised: March 11, 2014
Accepted: March 17, 2014
Published: March 17, 2014

dx.doi.org/10.1021/es405293u | Environ. Sci. Technol. 2014, 48, 4604−4612

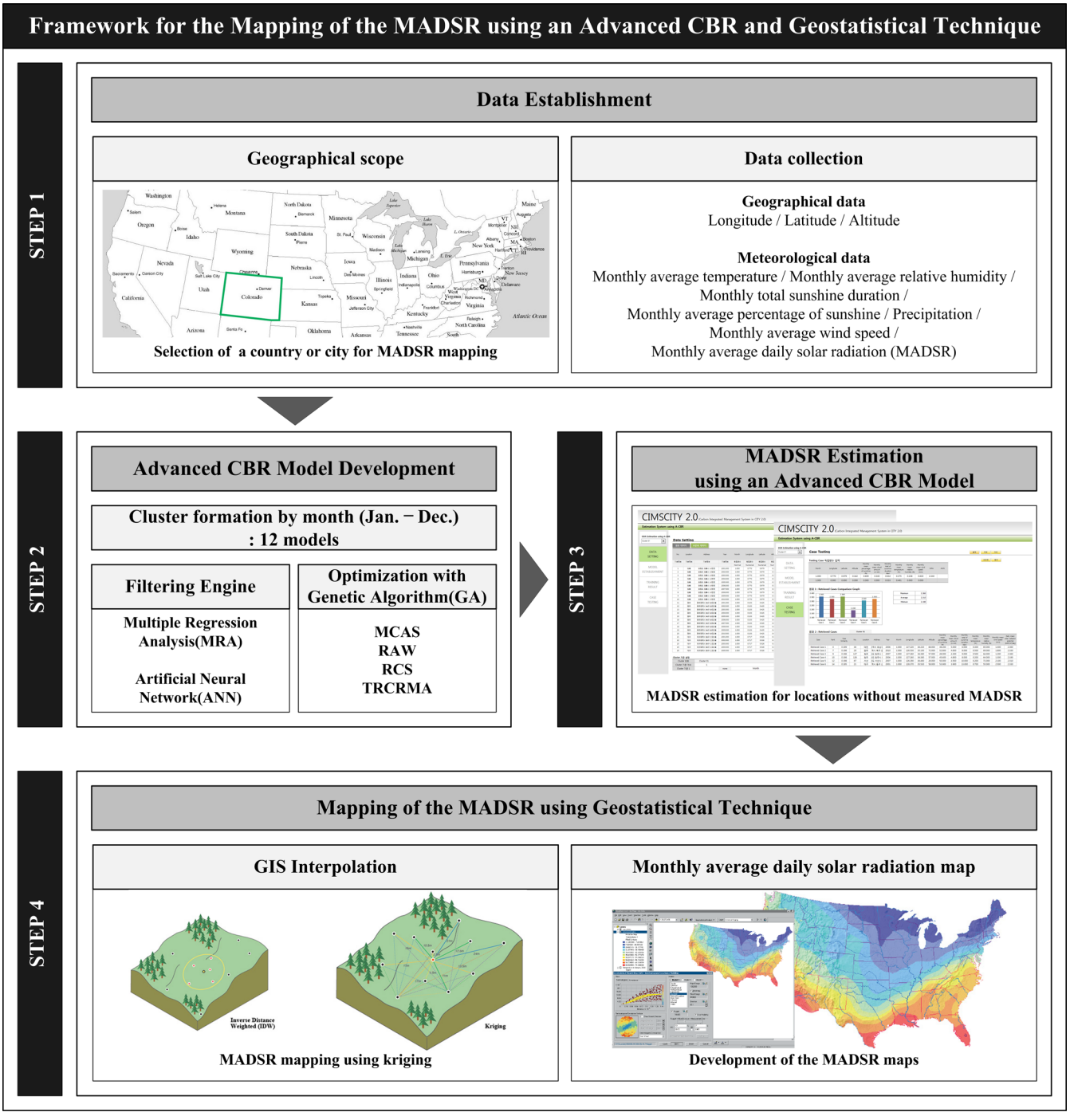

Figure 1. Framework for the mapping of the MADSR using an advanced CBR model and GIS.

such, spatial data mapping can become an effective method in terms of time and cost, and can improve one's understanding of the given information. Furthermore, spatial-data visualization using the geographic information system (GIS) can help decision makers to determine the current condition and future of the resources based on their decisions.[33,34] Therefore, the spatially continuous mapping of the MADSR has become a key tool in supporting the decision making for the effective distribution of PV systems. Regarding the mapping of the MADSR, the previous studies were conducted from various viewpoints.[35−49]

First, various studies using the GIS technique were conducted. To estimate the MADSR in Saudi Arabia, a monthly contour map using a geostatistical technique called *kriging* was developed. The application of the MADSR data from 41 regions showed that the mean percentage errors were between 0.5 and 1.7%, revealing the excellent performance of the methodology.[35] A GIS-based MADSR map was developed to estimate the MADSR distribution of Xinjiang in China. To reflect the complex topographic parameters of Xinjiang, it used the Solar Analyst of the "*ArcView GIS*" software as well as the Digital Elevation Model (DEM). The application of the MADSR data from 13 regions showed that the mean percentage errors were between 3.8% (July) and 12.2% (December), with an average of 7.1%.[36] The MADSR map in Catalonia was developed by using a computational, physically

dx.doi.org/10.1021/es405293u | *Environ. Sci. Technol.* 2014, 48, 4604−4612

based model, which was further interpolated with meteorological data. DEM was applied to "*MiraMon GIS*" software to take into account the astronomical, atmospheric, and geographic factors.[37]

Second, various studies using the artificial neural network (ANN) model were conducted. Sozen et al. (2004) developed an ANN model to estimate the MADSR in Turkey and to develop the MADSR map. The mean absolute percentage error (MAPE) and R^2 values of the testing data were 6.7 and 99.894%, respectively, showing the high estimation accuracy of the ANN model.[38] Fadare (2009) developed an ANN model to estimate the MADSR in Nigeria. The estimated MADSR was presented as a form of the MADSR map.[39] An ANN model and GIS were used to estimate the MADSR in Indonesia and to develop the MADSR map. The MAPE of the best result was 3.4%, showing its excellent performance.[40]

Third, various studies using satellite data were conducted. The MADSR in Italy was estimated using the "*SOLARMET*" physical model based on satellite data. It developed the MADSR map by summing the hourly MADSR data from the "*SOLARMET*" model.[41] Janjai (2010) estimated the MADSR in Thailand using "*MTSAT-1R*" satellite data and a satellite-based diffuse fraction model. The validity analysis of the model showed that the root-mean-square deviation and the mean bias were 16% and 1.6%, respectively.[42]

As such, various studies on the mapping of the MADSR have been conducted. Visualization of MADSR data requires as much data as possible, but as shown by the previous studies, there are insufficient locations with the measured MADSR data. Thus, it is difficult to develop an accurate MADSR map based only on the measured MADSR. Various previous studies were conducted to address this challenge; however, there are still the following limitations: (i) the accuracy of the MADSR map greatly depends on the accuracy of the raw data (e.g., DEM); (ii) the estimated MADSR data is simply showed on the MADSR map as a discrete map rather than a continuous map; (iii) the mapping of the MADSR using satellite data may not be applicable to all region (e.g., visible satellite data is not able to be used in mid or high latitude regions with snow in winter because it is not able to distinguish clouds from snow, and therefore, it is only suitable for tropical regions); and (iv) there is a lack of previous research study which can produce reliable MADSR data for developing more accurate MADSR map.

Therefore, this study estimated the MADSR at unmeasured locations through developing a MADSR estimation model which has high prediction accuracy. By integrating the measured and estimated MADSR data, this study proposed the framework for the mapping of the MADSR. An advanced case-based reasoning (CBR) model based on CBR method was used, which integrates ANN, multiregression analysis (MRA), and genetic algorithm (GA). Also, a geostatistical technique, *kriging*, was used as the methodology to develop the MADSR map.

The proposed framework consists of the following procedures (refer to Figure 1): (i) the geographic scope for the mapping of the MADSR is set, and the measured MADSR and meteorological data in the geographic scope are collected; (ii) using the collected data, the advanced CBR model is developed; (iii) using the advanced CBR model, the MADSR at unmeasured locations is estimated; and (iv) by applying the measured and estimated MADSR data to the GIS, MADSR map is developed. The proposed framework was applied to South Korea to conduct a practical validation. The framework proposed in this study can be applied to any other country in the global environment. It is expected that a more accurate and precise MADSR map can be developed using the proposed framework.

2. MATERIALS AND METHODS

2.1. Step 1: Data Establishment. *2.1.1. Definition of Variables.* The factors affecting the MADSR are identified and are used as the independent variables for the MADSR estimation model. Through extensive literature review and interviews with weather specialists, the factors affecting the MADSR are analyzed. They consist of geographic and meteorological factors. The geographic factors include location information like longitude, latitude, and altitude, while the meteorological factors include the monthly average temperature, monthly average relative humidity, monthly total sunshine duration, monthly average percentage of sunshine, precipitation, monthly average wind speed, and monthly average cloud amount.

2.1.2. Data Collection. Before the data collection, the country for which the MADSR map is to be developed is selected. Using the meteorological administration and NASA databases of the selected country, the geographic and meteorological data can be collected. To develop a precise MADSR map using the proposed framework, it is necessary to obtain the measured MADSR data from as many locations as possible or to estimate the MADSR data. Thus, in developing an MADSR estimation model, it is necessary to obtain the historical data which are collected for a minimum of five to ten years.

2.2. Step 2: Advanced CBR Model Development. On the basis of the data set, an advanced CBR model for the MADSR estimation is developed using the monthly geographic and meteorological data at the locations with the measured MADSR data.

First, clusters are formed by categorizing the data into 12 months. Each cluster consists of the historical data collected for a minimum of five to ten years, and the number of data in each cluster is calculated by multiplying "the number of locations with the measured MADSR data" by "the number of years with the measured MADSR data".

Second, the MADSR estimation model for each cluster is developed using the advanced CBR model. The advanced CBR model is a hybrid methodology of ANN, MRA, and GA based on the characteristics of the basic CBR methodology (i.e., retrieving cases with similar characteristics from historical cases). The model developed in this study combines the advantages of the existing methodologies and can therefore improve the prediction accuracy (which is the advantage of the ANN, MRA, and GA) and provide explanation on prediction results (which is the advantage of the CBR) at the same time.[50−57] By applying the advanced CBR model for developing MADSR estimation model, it provides more accurate and reliable estimation results of MADSR which is very crucial for MADSR mapping. In a previous research study conducted by Koo et al., an advanced CBR model was developed using 10-year measured MADSR data in 15 locations in South Korea (please refer to Koo et al.[3] if further understanding is required).

2.3. Step 3: MADSR Estimation Using an Advanced CBR Model. Using an advanced CBR model, the MADSR at unmeasured locations in the target country can be estimated. The geographic and meteorological data at unmeasured locations are used as the independent variables of the advanced

CBR model. The MADSR data estimated through this process, along with the measured MADSR, are used in developing the MADSR map using a geostatistical technique.

2.4. Step 4: Mapping of the MADSR Using a Geostatistical Technique. The MADSR map of the target country can be developed by integrating the measured and estimated MADSR data. Here, the software program called "*ArcMap 10.1*" of "*ArcGIS 10.1*" can be used. In particular, *kriging*, a function included in the extension of "*ArcMap 10.1*" which is a type of geographic information system interpolation (GISI), was used in this study.

An estimate at a point without the observed data can be derived by using the observed data at the nearby points. Such spatial interpolation technique is called GISI. There are two groups of spatial interpolation techniques: (i) deterministic and (ii) geostatistical. Both methods rely on the similarity between the observed data at the nearby points to create the surface. The former (e.g., inverse distance weighting (IDW)) uses mathematical functions for the spatial interpolation, while the latter (e.g., *kriging*) relies on both statistical and mathematical methods in order to create the surface and account for the uncertainty in prediction. The general formula for spatial interpolation is as follows:[58−63]

$$\hat{Z}(s_0) = \sum_{i=1}^{N} \lambda_i Z(s_i) \tag{1}$$

where, $\hat{Z}(s_0)$ is the estimated value at the unmeasured point (S_0); $Z(s_i)$ are the observed value at the measured points (S_i); N is the number of the measured points (S_i) surrounding unmeasured point (S_0); and λ_i are the weights assigned to each observed points (S_i).

In eq 1, the method for calculating the weights (λ_i) depends on the groups of spatial interpolation techniques. First, as its name implies, in the *IDW* method, the observed values of closer points are weighted more largely than those farther away. Thus, the *IDW* is referred to as a deterministic interpolation technique because it is directly based on the surrounding observed values. The formula for calculating the weights in the *IDW* technique can be expressed as follows:[59,62]

$$\lambda_i = d_{i0}^{-p} / \sum_{i=1}^{N} d_{i0}^{-p}, \quad \sum_{i=1}^{N} \lambda_i = 1 \tag{2}$$

where, λ_i are the weights assigned to each observed points (S_i in eq 1) (the sum of the weights (λ_i) is equal to (1); d_{i0} is the distance between the measure points (S_i in eq 1) and the unmeasured point (S_0 in eq 1); p is the power parameter influencing the weights (λ_i) for the measured points (S_i in eq 1) (as the distance (d_{i0}) becomes larger, the weight is decreased by a factor of p); and N is the number of the measured points (S_i in eq 1) surrounding unmeasured point (S_0 in eq 1).

Second, the *kriging* is referred to as a geostatistical interpolation technique, which is based on statistical models including autocorrelation (i.e., statistical relationships among the measured points (S_i in eq 1). The *kriging* is similar to the *IDW* in which it weights the observed value at the measured points (S_i in eq 1) to derive an estimated value for each unmeasured points (S_0 in eq 1). However, there is a difference for calculating the weights. While the *IDW* uses a simple algorithm based on distance (refer to eq 2), in the *kriging* method, the weights (λ_i in eq 1) are calculated based not only on the distance between the measured points (S_i in eq 1) and the unmeasured point (S_0 in eq 1) but also on the overall spatial arrangement among the measured points (S_i in eq 1). Namely, the *kriging* is based on the minimization the statistical expectation of the following:[59,63]

$$\varepsilon = (\hat{Z}(s_0) - \sum_{i=1}^{N} \lambda_i Z(s_i))^2 \tag{3}$$

where, ε is the random error with spatial dependence; $\hat{Z}(s_0)$ is the estimated value at the unmeasured point (S_0); $Z(s_i)$ are the observed value at the measured points (S_i); N is the number of the measured points (S_i) surrounding unmeasured point (S_0); and λ_i are the weights assigned to each observed points (S_i).

The *IDW* is suitable for clearly determining the regional differences from the microscopic view, while the *kriging* is suitable for determining the overall tendency of the region from the macroscopic view.[60,61] The framework proposed in this study involves developing the MADSR map of the whole country or city, and the *kriging* was determined to be more suitable for the study.

Meanwhile, there are many kinds of the *kriging* methods, such as ordinary, simple, universal, probability, indicator, and disjunctive *kriging*. Two *kriging* methods, ordinary and universal *kriging*, are provided in the extension called "*Spatial Analyst*" of "*ArcMap 10.1*". Ordinary *kriging*, which assumes the constant mean is unknown, is the most general and widely used method among many types of *kriging* method. However, universal *kriging* assumes that there is an overriding tendency in the data and should only be used when one can scientifically prove the trend in the data.[60] Therefore, this study aimed to propose a framework for mapping of MADSR of the target country using ordinary *kriging* method.

3. FRAMEWORK APPLICATION

This study proposed the framework for the mapping of the MADSR using an advanced CBR model and a geostatistical technique. To verify the validity of the proposed framework, a MADSR map targeting South Korea was developed, and a practical validation was conducted for the developed MADSR map.

In South Korea, Korea Meteorological Administration (KMA) collects and manages the meteorological data measured in 78 weather stations nationwide. As of 2011, the MADSR were measured in 24 regions of 78 weather stations by KMA. Supporting Information, SI, Table S1 shows the geographic description of the 78 weather stations in South Korea, and SI Figure S1 shows the mapping of their locations. In SI Figure S1, the 24 weather stations illustrated by the red circle show the station with both the measured MADSR and meteorological data while the other weather stations illustrated by pink circle show the station only with the measured meteorological data. The framework application for South Korea was conducted in the following four steps.

In step 1, the monthly geographic and meteorological data (including the MADSR) at the 24 locations with the measured MADSR data in South Korea (refer to the shaded areas in SI Table S1) for the last eight years (2004−2011) were collected.[64] On the basis of the collected data, geographic and meteorological data which could be measured in all the 78 weather stations in South Korea were selected as independent variables. Table 1 shows independent variables selected in this study. MADSR was used as the dependent variable.

Table 1. Target Variable and Independent Variables Affecting the Monthly Average Daily Solar Radiation

variables	attributes		detailed description
independent variable	geographical factor	longitude	°E
		latitude	°N
		altitude	m
	meteorological factor	monthly average temperature	°C
		monthly average relative humidity	%
		monthly total sunshine duration	hour
		monthly average percentage of sunshine	%
		precipitation	mm
		monthly average wind speed	m/s
target variable		monthly average daily solar radiation	kWh/m^2/day

In step 2, based on the data established in step 1, the advanced CBR model was developed for MADSR estimation on a monthly basis.

In step 3, using the advanced CBR model developed in step 2, the MADSR at the 54 unmeasured locations in South Korea were estimated. To estimate the MADSR with the advanced CBR model, the independent variables which were selected in step 1 are used.

In step 4, by combining the measured and estimated MADSR data, a MADSR map in South Korea was developed using a geostatistical technique called *kriging* in "*ArcGIG 10.1*" software program. For the validation of the developed MADSR map, the data in Daegu were used.

4. RESULTS AND DISCUSSION

4.1. Prediction Accuracy of an Advanced CBR Model. To verify the prediction accuracy of the advanced CBR model developed in framework application, the prediction accuracy of the advanced CBR model was compared with those of the ANN and MRA models, which were often used in the previous research studies, and the comparison results were analyzed. Also, through comparison with the CBR model, it was determined that the prediction accuracy of the advanced CBR model was improved. Table 2 shows the average prediction accuracy and the standard deviation of the prediction accuracy by the 12 MADSR estimation models. As shown in Table 2, the average prediction accuracy and standard deviation of the prediction accuracy for the developed advanced CBR model was 95.11% and 4.78%, respectively, showing very high consistency. Also, compared to the other models (ANN, MRA, and CBR models), its improvement was clear. First, in 11 of the 12 MADSR estimation models, the advanced CBR model showed higher prediction accuracy than MRA model. On average, the average prediction accuracy and the standard deviation of the prediction accuracy improved by 0.29 and 0.68%, respectively. Second, in 8 of the 12 MADSR estimation models, the advanced CBR model showed higher prediction accuracy than the ANN model. On average, the average prediction accuracy and the standard deviation of the prediction accuracy improved by 0.21 and 0.72%, respectively. Third, in all the models, the advanced CBR model had better prediction accuracy than the CBR model. On average, the average prediction accuracy and the standard deviation of the prediction accuracy improved by 2.66 and 2.40%, respectively.

In conclusion, it was determined that the advanced CBR model is an excellent methodology which can offer the advantage of the CBR model (which provides explanations of the prediction results based on historical cases) as well as the advantages of the ANN and MRA models (which guarantee excellent prediction accuracy).

4.2. MADSR Estimation Using an Advanced CBR Model. The advanced CBR model, proven to achieve high prediction accuracy, was used to estimate the MADSR at the 54 unmeasured locations in South Korea. As has been mentioned in step 1, KMA in South Korea collects and manages the meteorological data measured in the 78 weather stations nationwide. Among them, as of 2011, the MADSR data were only measured in 24 weather stations. Therefore, by applying the meteorological data collected in the other 54 weather stations to the advanced CBR model, the MADSR in each of the 54 stations could be estimated. SI Table S2 shows the estimated MADSR on a monthly basis in each of the 54 stations.

4.3. Mapping of the MADSR Using a Geostatistical Technique. The MADSR map was developed using *kriging*, a geostatistical technique in "*ArcMap 10.1*" of "*ArcGIS 10.1*". By combining the measured MADSR data and the estimated MADSR in step 3, the GIS-based MADSR map in South Korea was developed. Using the 77 data among a total of 78 regional data which were obtained from the combination of the 23 locations with the measured MADSR data and the 54 unmeasured locations, the MADSR map in South Korea was completed. To conduct the validation for framework application, the MADSR data of Daegu (refer to No. 15 in SI Table S1) among 24 locations with the measured MADSR data was excluded in developing the MADSR map in South Korea.

Table 2. Comparison of Predication Accuracy and Standard Deviation by Model

methodology[a]		Jan.	Feb.	Mar.	Apr.	May	Jun.	Jul.	Aug.	Sep.	Oct.	Nov.	Dec.	average
MRA	APA	93.66	95.00	95.75	95.96	95.77	95.28	93.60	95.06	95.39	95.47	93.84	92.99	94.81
	SDPA	6.78	4.85	4.06	4.30	4.53	4.13	5.22	4.35	4.17	4.77	8.40	9.89	5.45
ANN	APA	93.85	94.17	95.90	96.26	95.74	95.37	94.65	94.53	96.21	95.44	93.98	92.70	94.90
	SDPA	6.86	5.34	3.96	3.97	4.35	4.42	4.66	4.73	3.45	4.80	7.69	11.78	5.50
CBR	APA	91.56	92.84	93.65	94.38	92.77	92.73	90.47	92.67	92.62	94.05	90.60	91.05	92.45
	SDPA	7.78	5.00	6.13	6.02	6.90	7.05	8.92	6.07	7.10	5.40	10.24	9.47	7.17
advanced CBR	APA	94.04	94.96	95.86	96.19	95.91	95.44	94.25	95.14	96.05	95.75	94.03	93.67	95.11
	SDPA	6.31	4.63	3.67	3.79	4.31	3.86	4.31	3.85	3.26	4.50	7.79	7.06	4.78

[a]APA stands for the average prediction accuracy; and SDPA stands for the standard deviation of the prediction accuracy.

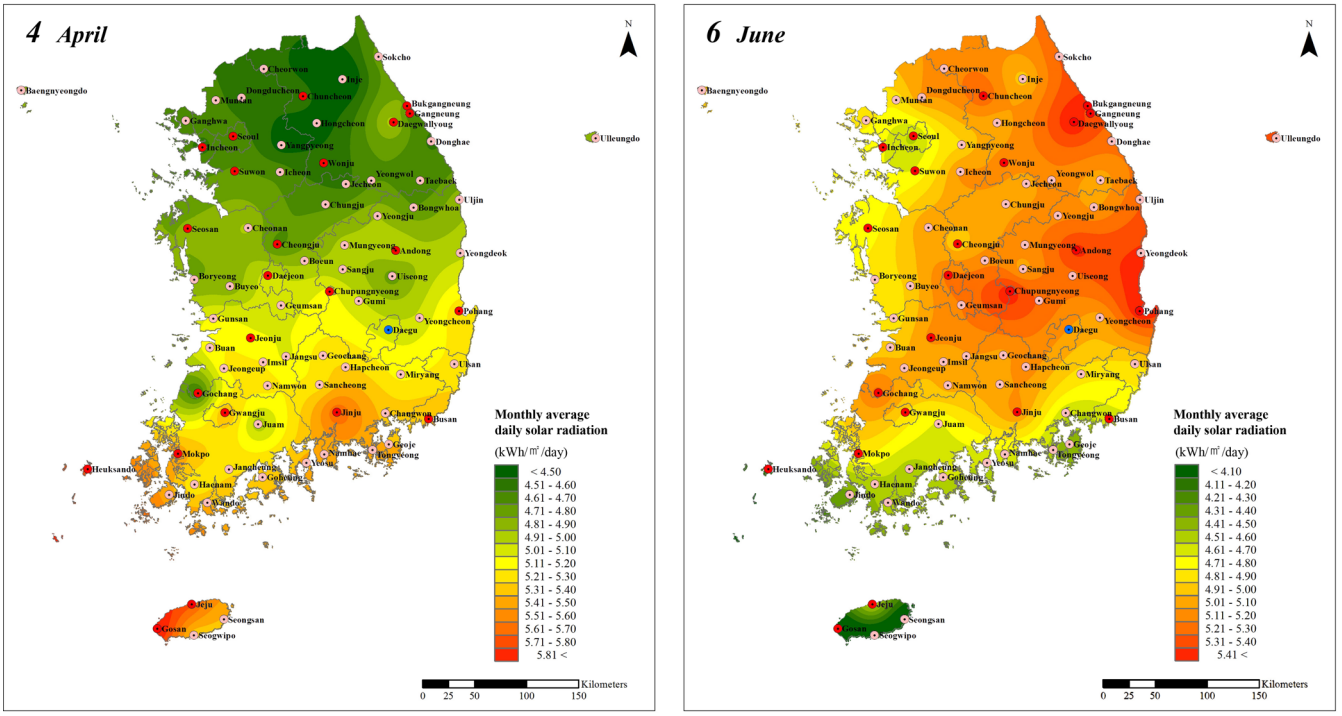

Figure 2. MADSR maps of April (left) and June (right) in South Korea.

Figure 2 and SI Figures S2−S6 are the MADSR map in South Korea which was developed through the above process. Each MADSR map was presented at the interval of 0.05 − 0.2 kWh/m^2/day on a monthly basis so that it can be easily used in estimating the MADSR at unmeasured locations. The locations illustrated by the red circle are the ones with the measured MADSR data, whereas those illustrated by pink circle are the ones whose MADSR was estimated using the advanced CBR model. Also, the location illustrated by blue circle (Daegu) is the one selected for validating the framework application.

As shown in Figure 2 and SI Figures S2−S6, the MADSR distribution in South Korea is diverse by month, and it generally tends to increase in the south. The MADSR maps in spring (March and April), summer (July), and winter (December and January) show that the MADSR increases in the southeast. However, the MADSR maps in fall (September and October) show that the MADSR increases in the southwest. In transitional seasons such as February, May, June, August, and November, the MADSR maps do not have a uniform pattern but are varied. In particular, the MADSR map in June shows that the MADSR increases in the northeast. Also, Jeju, the country's largest island, with an oceanic climate, shows a very different MADSR distribution pattern compared to the other regions.

According to Figure 2 and SI Figures S2−S6, the MADSR in South Korea varies from 1.24 to 6.10 kWh/m^2/day annually. The season with the largest MADSR is from March to June (spring to early summer). In particular, The MADSR in April is the largest (4.50−5.80 kWh/m^2/day). The season with the smallest MADSR is from November to February (late autumn to winter). In particular, the MADSR in December is the smallest (1.50−2.5 kWh/m^2/day).

In summary, by presenting such MADSR map, the MADSR at unmeasured locations can be estimated, and the seasonal and regional characteristics can be easily determined through the visual data on the MADSR distribution in South Korea.

4.4. Validation for the Framework Application. The validation for framework application was conducted with Daegu (the region illustrated by blue circle in Figure 2 and SI Figures S2−S6). In particular, the study aimed to verify the MADSR map (MADSRM-A), which was developed in this study by using a total of 77 regional data (consisting of the 23 locations with the measured MADSR data and the 54 locations with the estimated MADSR data). Toward this end, the MADSR map (MADSRM-B), which was developed only with the 23 measured MADSR data, was used as a comparison group.

4.4.1. Target Region for Validation. To verify the validity of the MADSR map in South Korea, one location in South Korea (Daegu, Gyeongsangbuk-do, South Korea) with the measured MADSR data was selected. One of the regions with the largest MADSR in South Korea, Daegu, is an erosion basin. Surrounded by high mountains, Daegu shows strong continental climates, being cold in winter and hot in summer, with the temperature going up to 40 °C, showing a large mean annual temperature range. As it is difficult for raincloud to pass through it, it is very dry, with an annual precipitation of around 900 mm. The summer season in Daegu shows the heat island phenomenon with concentric circular temperature distribution, and it is considered one of the hottest regions in the country.[65,66] Thus, the climate in Daegu is affected by its geographic location and topographic characteristics, for which reason it was considered to be suitable in order to verify the improvement effect of the MADSR map developed in this study.

4.4.2. Comparison of Prediction Accuracy between MADSRM-A and MADSRM-B. By comparing MADSRM-A and MADSRM-B, this study aimed to verify the prediction accuracy of MADSRM-A. First, this study estimated the MADSR in Daegu using MADSRM-A and MADSRM-B, respectively. To statistically compare the measured and estimated MADSR data, the MAPE was retrieved by calculating

dx.doi.org/10.1021/es405293u | Environ. Sci. Technol. 2014, 48, 4604−4612

Table 3. Comparison of Prediction Accuracy between MADSRM-A and MADSRM-B

region	class	monthly average daily solar radiation (kWh/m^2/day) Jan.	Feb.	Mar.	Apr.	May	Jun.	Jul.	Aug.	Sep.	Oct.	Nov.	Dec.	MAPE
Daegu	actual	2.98	2.97	4.78	4.90	4.79	5.06	4.09	3.60	3.83	3.30	2.03	2.02	
	MADSRM-A	2.84	3.13	4.87	5.05	4.91	5.10	4.13	3.71	3.85	3.48	2.12	2.34	
	error rate (%)	4.63	5.53	1.79	3.02	2.45	0.77	0.92	3.01	0.53	5.51	4.56	15.89	4.05
	MADSRM-B	3.12	3.18	5.15	5.31	5.00	5.36	4.57	3.80	4.15	3.65	2.22	2.51	
	error rate (%)	4.77	7.21	7.64	8.33	4.33	5.90	11.67	5.51	8.36	10.67	9.49	24.31	9.02

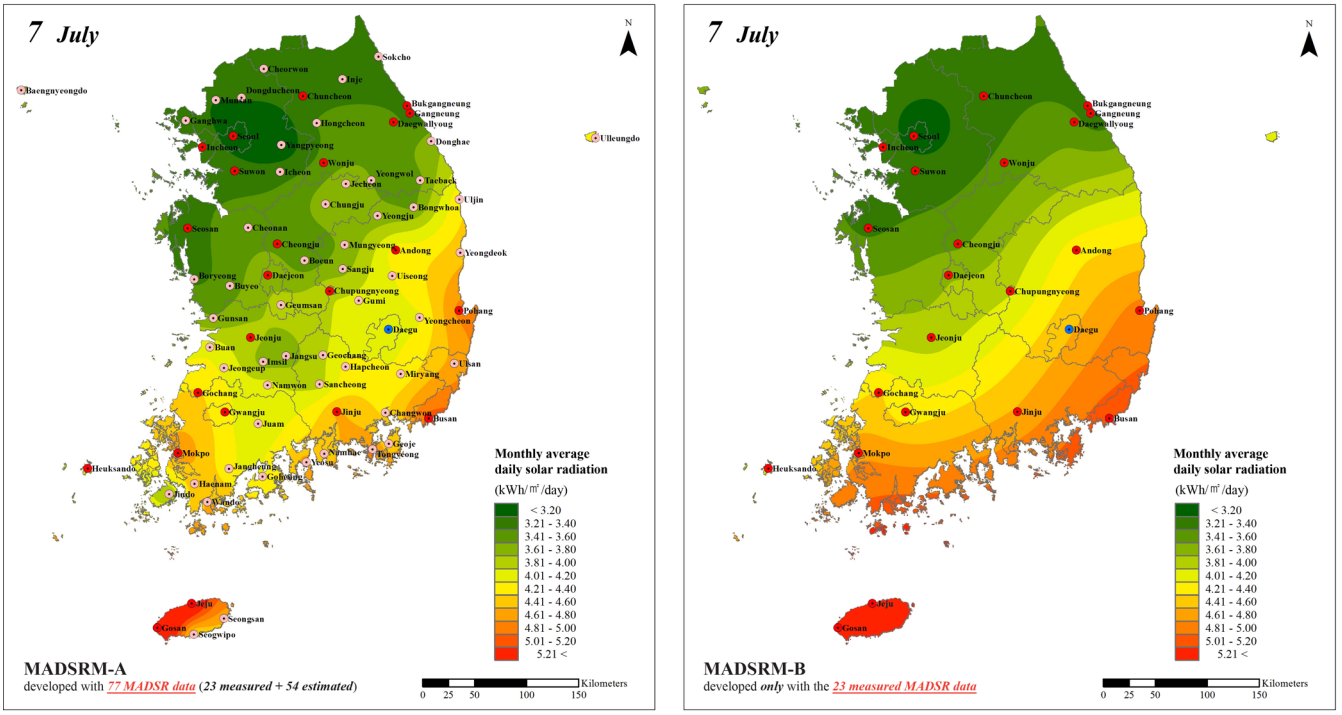

Figure 3. Comparison of MADSRM-A (left) and MADSRM-B (right) for July in South Korea.

the monthly error rate (ER). The following eqs 4 and 5 were used.

$$\mathrm{ER} = \left|\frac{\mathrm{AV} - \mathrm{EV}}{\mathrm{AV}}\right| \times 100 \tag{4}$$

$$\mathrm{MAPE} = \sum_{i=1}^{n} \left|\frac{\mathrm{AV}_i - \mathrm{EV}_i}{\mathrm{AV}_i}\right| \times \frac{1}{n} \times 100 \tag{5}$$

where, AV stands for the actual value (i.e., the measured MADSR data); EV stands for the estimated value (i.e., the estimated MADSR data); and n stands for the number of data.

Table 3 shows the results of the validation on a monthly basis, which were conducted by using MADSRM-A and MADSRM-B. Also, in order to identify the differences between them visually, Figure 3 shows the MADSRM-A and MADSRM-B in July.

As shown in Table 3, compared to MADSRM-B, the estimated MADSR in Daegu by using MADSRM-A was more accurate in all the months. First, in estimating the MADSR in Daegu by using MADSRM-A, the ER, compared to the measured MADSR in Daegu, was between 0.53 and 15.89% on a monthly basis, resulting in the MAPE at 4.05%. However, the estimated MADSR in Daegu using MADSRM-B showed an ER of 4.33−24.31% on a monthly basis in comparison with the measured MADSR, resulting in the MAPE at 9.02%. Thus, it concluded that MADSRM-A is superior to MADSRM-B in the overall prediction accuracy.

In comparing the results of the application of both MADSRM-A and MADSRM-B, in July, the ER between the measured MADSR data and the estimated MADSR in Daegu using MADSRM-A was 0.92%, and that using MADSRM-B was 11.67%, which showed the largest difference (10.75%) compared to the other months. Such huge difference in prediction accuracy using MADSRM-A and MADSRM-B can be explained in more detail in Figure 3. First, using MADSRM-A, in the southern part of South Korea, which has the largest MADSR in July, it shows that Mokpo, Jinju, Busan, and Pohang have larger MADSR than the surrounding regions, while Daegu, as an erosion basin, has a relatively small MADSR. However, using MADSRM-B, the overall MADSR in South Korea in July was found to have a tendency to increase from northwest to southeast, showing only the overall flow of the MADSR. In short, Figure 3 shows that MADSRM-A can demonstrate a precise MADSR distribution by geographic location compared to MADSRM-B.

Meanwhile, using MADSRM-A and MADSRM-B, the ER between the measured and estimated MADSR in Daegu in December was 15.89 and 24.31%, respectively, which were much larger than those in the other months. Compared to the measured MADSR in Daegu in December (as of 2011; 2.02 kWh/m^2/day), the estimated MADSR by MADSRM-A and

dx.doi.org/10.1021/es405293u | Environ. Sci. Technol. 2014, 48, 4604−4612

MADSRM-B were 2.34 and 2.51 kWh/m^2/day, respectively, which were relatively larger than the measured MADSR. This result can be attributed to the fact that the MADSR in December 2011 was considerably lower than the average MADSR in Daegu in December from 2004 to 2011 (2.31 kWh/m^2/day).

In conclusion, the MADSRM-A, which is developed by applying the proposed framework, can propose a more precise MADSR map compared to MADSRM-B. The MADSRM-A improves the prediction accuracy, and therefore, allows accurate MADSR estimation. Furthermore, due to the improved prediction accuracy and precise visualized data, the MADSRM-A can support accurate and effective decision making when introducing a PV system.

■ ASSOCIATED CONTENT

Supporting Information

Detailed data on the mapping of MADSR in South Korea, which were used in this study. This material is available free of charge via the Internet at http://pubs.acs.org.

■ AUTHOR INFORMATION

Corresponding Author

*Phone: 82-2-2123-5788; fax: 82-2-365-4668; e-mail: hong7@yonsei.ac.kr.

Notes

The authors declare no competing financial interest.

■ ACKNOWLEDGMENTS

This work was supported by the National Research Foundation of Korea (NRF) grant funded by the Korea government (MSIP; Ministry of Science, ICT & Future Planning) (No. NRF-2012R1A2A1A01004376).

■ REFERENCES

(1) *Climate Change 2007: Synthesis Report*; Intergovernmental Panel on Climate Change (IPCC), 2007.

(2) *Kyoto Protocol to the United Nations Framework Convention on Climate Change*; United Nations (UN), 1998.

(3) Koo, C.; Hong, T.; Lee, M.; Park, H. Estimation of the monthly average daily solar radiation using geographic information system and advanced case-based reasoning. *Environ. Sci. Technol.* **2013**, *47*, 4829−4839.

(4) Koo, C.; Park, S.; Hong, T.; Park, H. An estimation model for the heating and cooling demand of a residential building with a different envelope design using the finite element method. *Appl. Energy* **2014**, *115* (15), 205−215.

(5) Kim, J.; Hong, T.; Koo, C. Economic and environmental evaluation model for selecting the optimum design of green roof systems in elementary schools. *Environ. Sci. Technol.* **2012**, *46* (15), 8475−8483.

(6) Hong, T.; Kim, J.; Koo, C. LCC and LCCO$_2$ analysis of green roofs in elementary schools with energy saving measures. *Energy Buildings* **2012**, *45* (2), 229−239.

(7) *World Energy Outlook*; International Energy Agency (IEA): Paris, France, 2012.

(8) *Clean Energy Progress Report*; International Energy Agency (IEA): Paris, France, 2011.

(9) Hong, T.; Koo, C.; Kwak, T.; Park, H. An economic and environmental assessment for selecting the optimum new renewable energy system for educational facility. *Renew. Sust. Energy Rev.* **2014**, *29* (1), 286−300.

(10) Hong, T.; Koo, C.; Kwak, T. Framework for the implementation of a new renewable energy system in an educational facility. *Appl. Energy* **2013**, *103* (3), 539−551.

(11) *Renewable Energy Market and Policy Trends in IEA Countries*; International Energy Agency (IEA): France, 2009.

(12) *Renewables 2011: Global Status Report*; Renewable Energy Policy Network for the 21st Century (REN21): Paris, France, 2011.

(13) *Trends in Photovoltaic Applications: Survey Report of Selected IEA Countries between 1992 and 2011*; International Energy Agency PVPS (IEA PVPS): Switzerland, 2012.

(14) *2010 Solar Technologies Market Report*; National Renewable Energy Laboratory (NREL): Colorado, USA, 2011.

(15) *Global Market Outlook for Photovoltaics until 2015*; European Photovoltaic Industry Association (EPIA): Brussels, Belgium, 2011.

(16) Hong, T.; Koo, C.; Lee, M. Estimating the loss ratio of solar photovoltaic electricity generation through stochastic analysis. *J. Constr. Eng. Project Manage.* **2013**, *3* (3), 23−34 (Special Issue: Best Paper Award and Selected papers from the 5th International Conference on Construction Engineering and Project (ICCEPM 2013))..

(17) Koo, C.; Hong, T.; Park, H.; Yun, G. Framework for the analysis of the potential of the rooftop photovoltaic system to achieve the net-zero energy solar buildings. *Prog. Photovolt.: Res. Appl.* **2014**, in press.

(18) Geraldi, E.; Romano, F.; Ricciardelli, E. An advanced model for the estimation of the surface solar irradiance under all atmospheric conditions using MSG/SEVIRI data. *IEEE Trans. Geosci. Remote Sens.* **2012**, *50* (8), 2934−2953.

(19) Badescu, V. Correlations to estimate monthly mean daily solar global radiation: Application to Romania. *Energy* **1999**, *24* (10), 883−893.

(20) Chegaar, M.; Chibani, A. Global solar radiation estimation in Algeria. *Energy Convers. Manage.* **2001**, *42* (8), 967−973.

(21) Ashhab, M. S. S. Optimization and modeling of a photovoltaic solar integrated system by neural networks. *Energy Convers. Manage.* **2008**, *49* (11), 3349−3355.

(22) Reddy, K. S.; Ranjan, M. Solar resource estimation using artificial neural networks and comparison with other correlation models. *Energy Convers. Manage.* **2003**, *44* (15), 2519−2530.

(23) Cano, D.; Monget, J. M.; Albuission, M.; Guillard, H.; Regas, N.; Wald, L. A method for the determination of the global solar radiation from meteorological satellite data. *Solar Energy* **1986**, *37* (1), 31−39.

(24) Gastli, A.; Charabi, Y. Solar electricity prospects in Oman using GIS-based solar radiation maps. *Renew. Sust. Energy Rev.* **2010**, *14*, 790−797.

(25) Mohandes, M.; Rehman, S.; Halawani, T. O. Estimation of global solar radiation using artificial neural networks. *Renew. Energy* **1998**, *14* (1−4), 179−184.

(26) Alawi, S. M.; Hinai, H. A. An ANN-based approach for predicting global radiation in locations with no direct measurement instrumentation. *Renew. Energy* **1998**, *14* (1−4), 199−204.

(27) Dorvio, A. S. S.; Jervase, J. A.; Al-Lawati, A. Solar radiation estimation using artificial neural networks. *Appl. Energy* **2002**, *71* (4), 307−319.

(28) Sozen, A.; Arcaklýogblub, E.; Ozalpa, M.; Agclarc, N. C. Forecasting based on neural network approach of solar potential in Turkey. *Renew. Energy* **2005**, *30* (7), 1075−1090.

(29) Mubiru, E. J.; Banda, K. B. Estimation of monthly average daily global solar radiation using artificial neural networks. *Solar Energy* **2008**, *82* (2), 181−187.

(30) Behrang, M. A.; Assareh, E.; Ghanbarzadeh, A.; Noghrehabadi, A. R. The potential of different artificial neural network (ANN) techniques in daily global solar radiation modeling based on meteorological data. *Solar Energy* **2010**, *84* (8), 1468−1480.

(31) Súri, M.; Hofierka, J. A new GIS-based solar radiation model and its application to photovoltaic assessments. *Trans. GIS* **2004**, *8* (2), 175−190.

(32) Janjai, S.; Pankaewa, P.; Laksanaboonsong, J.; Kitichantaropas, P. Estimation of solar radiation over Cambodia from long-term satellite data. *Renew. Energy* **2011**, *36* (4), 1214−1220.

(33) Pundt, H.; Brinkkotter-Runde, K. Visualization of spatial data for field based GIS. *Comput. Geosci.* **2000**, *26* (1), 51−56.

(34) Latu, S. Sustainable development: The role of GIS and visualisation. *Electron. J. Inform. Syst. Dev. Countries* **2000**, *38* (5), 1−17.
(35) Rehmana, S.; Ghori, S. G. Spatial estimation of global solar radiation using geostatistics. *Renew. Energy* **2000**, *21* (3−4), 583−605.
(36) Li, J. Spatial distribution of incoming potential solar radiation based on Solar Analyst model and DEM in Xinjiang, China. *Geoinformatics 2008 and Joint Conference on GIS and Built Environment: Advanced Spatial Data Models and Analyses* **2008**, 71462M1−71462M8.
(37) Pons, X.; Ninyerola, M. Mapping a topographic global solar radiation model implemented in a GIS and refined with ground data. *Int. J. Climatol.* **2008**, *28* (13), 1821−1834.
(38) Sozen, A.; Arcaklioglu, E.; Ozalp, M.; Kanit, E. G. Use of artificial neural networks for mapping of solar potential in Turkey. *Appl. Energy* **2004**, *77* (3), 273−286.
(39) Fadare, D. A. Modelling of solar energy potential in Nigeria using an artificial neural network model. *Appl. Energy* **2009**, *86* (9), 1410−1422.
(40) Rumbayan, M.; Abudureyimu, A.; Nagasaka, K. Mapping of solar energy potential in Indonesia using artificial neural network and geographical information system. *Renew. Sust. Energy Rev.* **2012**, *16* (3), 1437−1449.
(41) Cogliani, E.; Ricchiazzi, P.; Maccari, A. Generation of operational maps of global solar irradiation on horizontal plan and of direct normal irradiation from Meteosat imagery by using SOLARMET. *Solar Energy* **2008**, *82* (6), 556−562.
(42) Janjai, S. A method for estimating direct normal solar irradiation from satellite data for a tropical environment. *Solar Energy* **2010**, *84* (9), 1685−1695.
(43) Janjai, S.; Laksanaboonsong, J.; Nunez, M.; Thongsathitya, A. Development of a method for generating operational solar radiation maps from satellite data for a tropical environment. *Solar Energy* **2005**, *78* (6), 739−751.
(44) Hu, Z. M.; Wu, J. P.; Wu, B.; Shu, S.; Yu, B. L. Simulating and mapping the variations of solar radiation at the Lujiazui region of Shanghai using airborne LiDAR data. *Key Eng. Mater.* **2012**, *500*, 511−516.
(45) Mohandes, M.; Rehman, S. Global Solar Radiation Maps of Saudi Arabia. 2010 International Conference on Renewable Energy (ICRE) 2010.
(46) Herbst, D. Solar mapping: Demystifying solar potential. *Renew. Energy Focus*, **2009**, July/August, pp 32−35.
(47) Winslow, J. C.; Raymond Hunt, E., Jr; Piper, S. C. A globally applicable model of daily solar irradiance estimated from air temperature and precipitation data. *Ecol. Model.* **2001**, *143*, 227−243.
(48) Thornton, P. E.; Running, S. W. An improved algorithm for estimating incident daily solar radiation from measurements of temperature, humidity, and precipitation. *Agric. Forest Meteorol.* **1999**, *93*, 211−228.
(49) López, G.; Batlles, F. J.; Tovar-Pescador, J. Selection of input parameters to model direct solar irradiance by using artificial neural networks. *Energy* **2005**, *30*, 1675−1684.
(50) Hong, T.; Koo, C.; Kim, H.; Park, H. Decision support model for establishing the optimal energy retrofit strategy for existing multi-family housing complexes. *Energy Policy* **2014**, *66*, 157−169.
(51) Hong, T.; Koo, C.; Lee, S. Benchmarks as a tool for free allocation through comparison with similar projects: Focused on multi-family housing complex. *Appl. Energy* **2014**, *114* (2), 663−675.
(52) Hong, T.; Koo, C.; Kim, H. A decision support model for improving a multi-family housing complex based on CO_2 emission from electricity consumption. *J. Environ. Manage.* **2012**, *112* (15), 67−78.
(53) Hong, T.; Koo, C.; Jeong, K. A decision support model for reducing electric energy consumption in elementary school facilities. *Appl. Energy* **2012**, *95* (7), 253−266.
(54) Hong, T.; Koo, C.; Park, S. A decision support model for improving a multi-family housing complex based on CO_2 emission from gas energy consumption. *Building Environ.* **2012**, *52* (6), 142−151.
(55) Koo, C.; Hong, T.; Hyun, C. The development of a construction cost prediction model with improved prediction capacity using the advanced CBR approach. *Int. J. Expert Syst. Appl.* **2011**, *38* (7), 8597−8606.
(56) Koo, C.; Hong, T.; Hyun, C.; Park, S.; Seo, J. A study on development of a cost model based on the owner's decision making at the early stages of a construction project. *Int. J. Strat. Property Manage.* **2010**, *14* (2), 121−137.
(57) Koo, C.; Hong, T.; Hyun, C.; Koo, K. A CBR-based hybrid model for predicting a construction duration and cost based on project characteristics in multi-family housing projects. *Can. J. Civil Eng.* **2010**, *37* (5), 739−752.
(58) Burrough, P. A.; McDonnell, R. A. *Principles of Geographical Information Systems*; Oxford University Press: Oxford, U.K., 1998.
(59) Johnston, K.; Ver Hoef, J.; Krivoruchko, K.; Lucas, N. *Using ArcGIS Geostatistical Analyst*; ESRI: USA, 2001.
(60) McCoy, J.; Johnston, K. *Using ArcGIS Spatial Analyst*; ESRI: USA, 2001.
(61) GIS Interpolation (IDW, Kriging); http://www.biz-gis.com/index.php?document_srl=12477&mid=paper.
(62) Inverse Distance Weighting (IDW) from Wikipedia, the free encyclopedia; http://en.wikipedia.org/wiki/Inverse_distance_weighting.
(63) Kriging from Wikipedia, the free encyclopedia; http://en.wikipedia.org/wiki/Kriging.
(64) *Monthly Weather Report (from January 2004 to December 2011)*; Korea Meteorological Administration (KMA): Seoul, South Korea, 2004−2011.
(65) *The Geography of Korea*; National Geographic Information Institute (NGII): Suwon, South Korea, 2010.
(66) *The Climate Atlas of Korea (1981∼2010)*; Korea Meteorological Administration (KMA): Seoul, South Korea, 2012.